Journal of Engineering Physics and Thermophysics, Vol. 82, No. 2, 2009

MATHEMATICAL MODELING OF THE HEATING AND MELTING OF THE METAL CHARGE IN AN ELECTRIC-ARC STEEL-MAKING FURNACE

Yu. A. Stankevich,[a] V. I. Timoshpol'skii,[b] N. V. Pavlyukevich,[a] M. G. German,[c] and P. S. Grinchuk[a]

UDC 669.18

A mathematical model has been developed and an algorithm of calculation of heat- and mass-transfer processes in heating and melting of metal scrap in an electric-arc steel-making furnace has been created. The results of numerical modeling of the dynamics of melting of metal scrap in this furnace have been given.

Keywords: *metal scrap, melting, electric-arc steel-making furnace, molten bath, radiation fluxes, heat exchange, mathematical model.*

Introduction. The complexity of the mathematical model of heating and melting of metal scrap in an electric-arc steel-making furnace is due to the fact that heat- and mass-transfer processes in phase transformations occur simultaneously in two different media; at the same time, there occurs between them a constant heat and mass exchange in the case of moving boundaries of the media [1]. Furthermore, both media in the electric-arc steel-making furnace are heterogeneous (multiphase).

To describe the heat and mass transfer in the electric-arc steel-making furnace, let us use the phenomenological theory of interpenetrating continua [2, 3], in which the system of equations for a heterogeneous medium is written on the basis of the laws of conservation of mass, momentum, and energy for each phase. To close this system of equations, additional assumptions are involved regarding the quantities describing interphase interactions. The presence of phase transitions (melting, evaporation) in both media and of moving boundaries of these media, through which there occurs an intense heat and mass transfer, suggests a formulation of the problem as a conjugate one, i.e., it is necessary to use as a basis the system of equations of conjugate heat and mass transfer in the working chamber of the electric-arc steel-making furnace.

The overwhelming part of the energy is produced by the arcs as radiation. Therefore, great importance is attached to the calculation of the lateral flows of radiation (gradients) of the arcs and the electrode that determine the heating of the melt and the melting of the lateral wall of the charge in the region adjacent to the surface of the melt. It is also necessary to take into account an additional contribution of the radiation of the graphite electrode being heated, especially during the heating of the charge in the region of the well when these regions are shielded from the arc's radiation by the electrode.

System of Equations in the Region of the Metal Charge. We perform calculations with account taken of the presence of a marsh in the furnace, i.e., a melted mass of metal h_{m0}-high that has remained from a previous melting (Fig. 1) [1]. In the region occupied by the metal charge, blowing with heated gas is expected, i.e., we have a two-phase system solid scrap particles–gas. The system of energy equations for each phase has the form

$$\varepsilon\bar{\rho}_g C_{pg}\frac{\partial T_g}{\partial \tau}+\bar{\rho}_g w_z C_{pg}\frac{\partial T_g}{\partial z}=-\alpha_{v,\text{eff}}(T_g-T_s)+\varepsilon\frac{\bar{\rho}_g v_g C_{pg}(T_*-T_g)}{(1/2)R}, \tag{1}$$

$$(1-\varepsilon)\bar{\rho}_s C_{ps,\text{eff}}\frac{\partial T_s}{\partial \tau}=\alpha_{v,\text{eff}}(T_g-T_s)+\frac{\partial}{\partial z}\left(\lambda_{s,\text{eff}}\frac{\partial T_s}{\partial z}\right)+\frac{1}{r}\frac{\partial}{\partial r}\left(\lambda_{s,\text{eff}} r\frac{\partial T_s}{\partial r}\right)+Q^{\text{chem}}, \tag{2}$$

[a]A. V. Luikov Heat and Mass Transfer Institute, National Academy of Sciences of Belarus, 15 P. Brovka Str., Minsk, 220072, Belarus; email: pnv@hmti.ac.by; [b]"Eurofinance Ltd." Company, Kiev; [c]Belarusian Institute of Thermal-Power Engineering, Minsk. Translated from Inzhenerno-Fizicheskii Zhurnal, Vol. 82, No. 2, pp. 227–241, March–April, 2009. Original article submitted July 7, 2008.

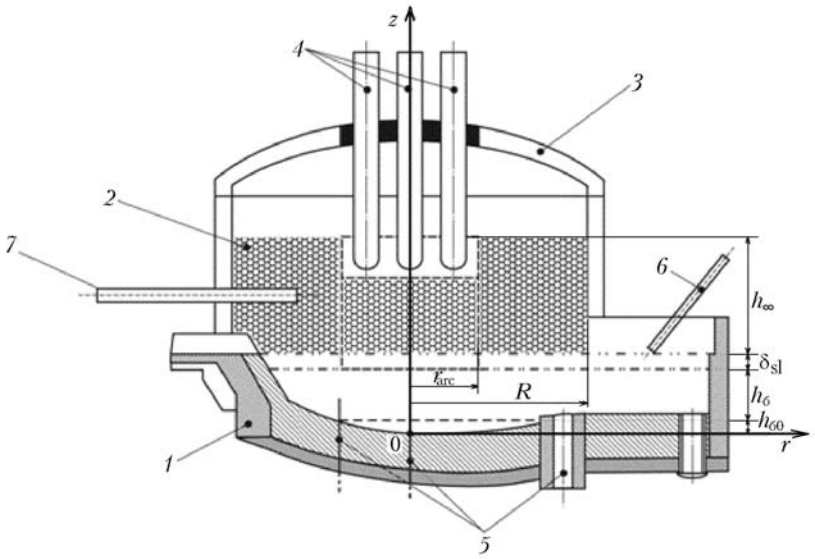

Fig. 1. Electric-arc steel-making furnace: 1) furnace bottom; 2) metal charge; 3) furnace roof; 4) electrodes; 5) bottom lances; 6) erker manipulator lance; 7) manipulator lance.

where $h_m(\tau) < z < h_s(\tau)$, $0 < r < R$; ε is porosity which is considered to be constant;

$$w_z = \varepsilon v_{zg} = \varepsilon \frac{v_g}{\frac{1}{2}R}(z - h_m); \tag{3}$$

$$\lambda_{s,eff}(T) = \lambda_{s0}(T)(1-\varepsilon) + \frac{32}{9}\sigma d_s \frac{\varepsilon^2}{1-\varepsilon} T_s^3; \tag{4}$$

$$C_{ps,eff} = \begin{cases} C_{ps}, & T < T_{sol}; \\ C_{ps} + \dfrac{Q}{T_{liq} - T_{sol}}, & T_{sol} < T < T_{liq}; \\ 0, & T > T_{liq}; \end{cases} \tag{5}$$

$\mathbf{w} = \varepsilon \mathbf{v}_g$ is the filtration velocity and $\mathbf{v}_g$ is determined from the total flow-rate of the gas in the burners. The last term in (4) is the radiant thermal conductivity in a high-porosity scrap charge [3]. The effective coefficient of internal heat exchange $\alpha_{v,eff}$ is determined from the following relation:

$$\frac{1}{\alpha_{v,eff}} = \frac{1}{\alpha_v} + \frac{1}{\alpha_{v,in}}, \tag{6}$$

where $\alpha_{v,in} = 4\pi^2\lambda_s(1-\varepsilon)/d_s^2$ is determined by the process of heat conduction inside a solid scrap particle; α_v is the coefficient of internal heat exchange between the skeleton of the porous body and the gas, whose value can be taken from the literature (see, e.g., [5] where $\alpha_v \approx 70$–300 W/(m^3·K)) or be calculated from the formula [3, 6]:

$$\alpha_v = \frac{6(1-\varepsilon)}{d_s^2}\lambda_g\left(2 + 1.1\mathrm{Pr}^{1/3}\mathrm{Re}^{0.6}\right), \quad \mathrm{Re} = \frac{\overline{\rho}_g d_s w}{\mu_g}, \quad \mathrm{Pr} = \frac{\mu_g C_{pg}}{\lambda_g}.$$

The heat source Q^{chem} in (2) reflects the process of scaling when iron is oxidized in heating of the scrap:

$$Q^{\text{chem}} = \rho_{\text{FeO}} \frac{\Delta H}{\overline{M}_{\text{s}}} S \frac{dX}{d\tau} (1-\varepsilon), \quad X = \left(\alpha_m k_m^0 \tau\right)^{1/2}, \quad \tau = \int_0^{\tau} \exp\left(-\frac{E}{\overline{R}T(\xi)}\right) d\xi, \tag{7}$$

where

$$E = \begin{cases} 138{,}070 \text{ J/mole}, & T < 1000^{\circ}\text{C}; \\ 157{,}540 \text{ J/mole}, & T > 1000^{\circ}\text{C}; \end{cases} \quad k_m^0 = \begin{cases} 37 \text{ kg/(m}^4\cdot\text{sec)}, & T < 1000^{\circ}\text{C}; \\ 304.7 \text{ kg/(m}^4\cdot\text{sec)}, & T > 1000^{\circ}\text{C}; \end{cases}$$

ΔH = 261,000 J/mole, $\alpha_m = 1.8\cdot10^{-6}$ m^6/kg^2, and $\rho_{\text{FeO}} = 5.6\cdot10^3$ kg/m^3; $\overline{M}_{\text{s}}$ is the molecular weight of FeO.

In this model, it is assumed that in the process of melting, liquid metal flows down into the marsh, i.e., the liquid phase is absent from the region of the scrap ($h_{\text{m}}(\tau) < z < h_{\text{s}}(\tau)$) but the change in the volume of the fluid bath due to the flowing-down fluid is taken into account. For this purpose, we write an expression for the averaged (over r) velocity of motion of the upper boundary of the marsh $h_{\text{m}}(\tau)$:

$$\overline{\rho}_{\text{f}} \frac{d\Delta h_{\text{m}}}{d\tau} = \frac{2(1-\varepsilon)\overline{\rho}_{\text{s}} \int_{h_{\text{m}}}^{h_{\text{s}}} \int_0^R A_0(r, z, \tau)\, r dr dz}{\varepsilon R^2} + \frac{\left(\overline{\rho}_{\text{s}}^{\text{m}} - \overline{\rho}_{\text{f}}^{\text{m}}\right) \int_{V_{\text{m}}} A_0^{\text{m}} dV_{\text{m}} \varepsilon_{\text{s}}^{\text{m}}}{\varepsilon_{\text{f}}^{\text{m}} \pi R^2}, \tag{8}$$

where

$$A_0 = \begin{cases} 0, & T < T_{\text{sol}}; \\ \dfrac{1}{T_{\text{liq}} - T_{\text{sol}}} \dfrac{\partial T_{\text{s}}(r, z, \tau)}{\partial \tau}, & T_{\text{sol}} < T < T_{\text{liq}}; \\ 0, & T_{\text{liq}} < T; \end{cases} \quad A_0^{\text{m}} = \begin{cases} 0, & T < T_{\text{sol}}^{\text{m}}; \\ \dfrac{1}{T_{\text{liq}}^{\text{m}} - T_{\text{sol}}^{\text{m}}} \dfrac{\partial T^{\text{m}}}{\partial \tau}, & T_{\text{sol}}^{\text{m}} < T < T_{\text{liq}}^{\text{m}}. \\ 0, & T > T_{\text{liq}}^{\text{m}} \end{cases}$$

Relation (8) actually corresponds to the continuity equation for the solid phase in the region of scrap, the quantity A_0 reflects the amount of the molten scrap at a given instant, and the last term on the right in (8) shows the change in the fluid volume because of the difference in the densities of the fluid and the scrap. It should be noted that in a numerical realization of the mathematical model considered the rise in the level of the marsh is accounted for in a discrete manner. The computational cells of the melted charge are transferred to the marsh, ensuring a rise in its level. Naturally, the cells that have not melted yet and are lying higher "fall down" onto the surface of the marsh. At this time, the layer is being filled with account taken of the conservation of mass and enthalpy.

The upper boundary of scrap h_{s} is a complex function of the coordinates and time. Therefore, $h_{\text{s}}(r, z, \tau)$ can approximately be determined from the isotherm $T = T_{\text{liq}}$ or in the approximation of a flat surface:

$$\overline{\rho}_{\text{s}} \frac{d\Delta h_{\text{s}}}{d\tau} = \frac{2(1-\varepsilon)\overline{\rho}_{\text{s}} \int_{h_{\text{m}}}^{h_{\text{s}}} \int_0^R A_0 r dr dz}{R^2} + \frac{\varepsilon_{\text{s}}^{\text{m}} \rho^{\text{m}} \int_{V_{\text{m}}} A_0^{\text{m}} dV_{\text{m}}}{\pi R^2}. \tag{9}$$

Formation of a Well under the Arc. It is possible to obtain an expression for the velocity of descent of the solid phase directly under the arc from the general equation of motion of the solid phase in a heterogeneous medium [2] through its simplification. Due to the fusion of solid-phase particles and the reduction of the volume of the charge under the well, the solid phase will descend rather quickly. An approximate equation for the descending velocity of the scrap in the region under the arc takes the form

$$\frac{dv_{sz}}{dz} = \overline{A}_0, \tag{10}$$

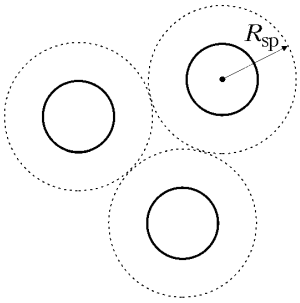

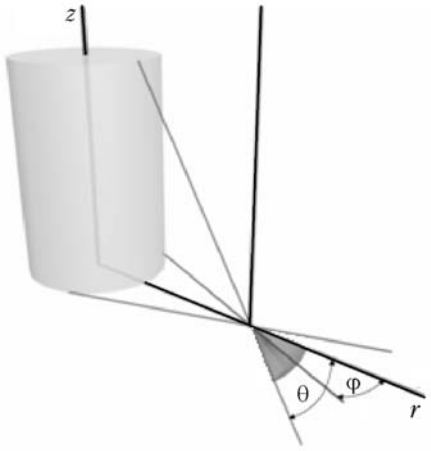

Fig. 2. Arrangement of hot spots of the electrodes.

Fig. 3. Determination of the z component of the radiation flux.

$$\overline{A}_0 = \begin{cases} 0\,, & T < T_{sol}\,; \\ \dfrac{1}{T_{liq} - T_{sol}} \dfrac{\partial T_s\,(z, T)}{\partial \tau}\,, & T_{sol} < T < T_{liq}\,, \quad 0 < r < R_{arc}\,. \\ 0\,, & T_{liq} < T \end{cases} \tag{11}$$

As calculations have shown, the initial phase of formation of a well is quite short and lasts a few minutes (depending on the temperature of the arc). After the formation of a well, the arc "descends" on the surface of the marsh and the melting of the charge in this region is ensured by the lateral radiation of the arc and of the electrode. In numerical realization of the calculation program, further expansion of the well is determined by the mechanism of vertical "collapse" of the upper layer of the charge. The motion of the charge in the process of the formation of a well is described in a natural manner, i.e., the arc is always tied to the bottom of the well or to the surface of the molten bath.

Radiation Fluxes of Arc Emission. Let us determine the equivalent radius R_{arc} of the spot of a heat source formed as a result of the action of three arcs. We evaluate R_{arc} on the basis of [7]. In calculating the density of the heat flux by radiation on the metal surface in a three-electrode electric-arc steel-making furnace during the period of fluid bath, it is assumed that the arc ($2h_{arc}$-long) is considered as a point source of radiation located in the middle of the distance (h_{arc}) between the surfaces of the bath mirror and the electrode end. The distribution of the heat-flux density reveals the presence of a pronounced maximum in the region on the surface of the bath located under the electrodes. These three circular regions symmetric about the vertical axes of the electrodes, whose area accounts for 90% of the entire energy emitted onto the bath, are called hot spots (Fig. 2). The radius of the hot spots R_{sp} is virtually independent of the electrode's radius and is accurately determined by the length of the arc $2h_{arc}$.

As is shown in [7], in the investigated range of variation in the parameters for furnaces with capacities of 10, 50, and 100 tons, one can use a dependence that makes it possible (for engineering calculations) to quite accurately determine the radii of the hot spots R_{sp}:

$$R_{sp} = 7 + 3\,(2h_{arc})\,. \tag{12}$$

Then the equivalent radius of the arc R_{arc} can be determined from the relation $\pi R_{arc}^2 = 3\pi R_{sp}^2$, i.e.,

$$R_{arc} = R_{sp}\sqrt{3}\,. \tag{13}$$

For example, with a length of the arc of $2h_{arc}$ = 0.1 m (12) yields R_{sp} = 0.37 m, and (13) yields R_{arc} = 0.64 m in the case of a three-electrode furnace. We also assume that $h_{arc,eff} = \sqrt{3} \cdot 2h_{arc}$ = 0.17 m.

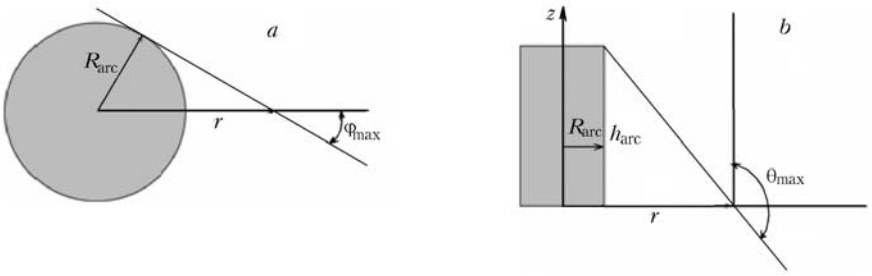

Fig. 4. Determination of the limits of integration by the angle φ (a) and by the angle θ (b).

Let us consider the electric arc as a source of heating of the charge and the molten bath. It is also the main source of heating of the graphite electrode. The integral radiation flux is determined as

$$\mathbf{S} = \int_0^{\infty} \mathbf{S}_\nu d\nu\,, \quad \mathbf{S}_\nu = \int_{(4\pi)} \mathbf{I}_\nu \boldsymbol{\Omega} d\boldsymbol{\Omega} = \int_0^{2\pi} d\varphi \int_0^{\pi} \mathbf{I}_\nu (\theta, \varphi) \cos(\theta) \sin(\theta)\, d\theta\,, \tag{14}$$

here, we have

$$S_r (r_0, z_0) = \int_0^{2\pi} d\varphi \int_0^{\pi} \cos\varphi \sin^2\theta I_\nu d\theta\,, \quad S_z (r_0, z_0) = \int_0^{2\pi} d\varphi \int_0^{\pi} \cos\theta \sin\theta I_\nu d\theta\,.$$

The spectrum-integral equilibrium intensity is equal to

$$I_0 = \frac{S_0}{\pi} = \frac{\sigma T_{arc}^4}{\pi}\,.$$

The radiation power of the arc is a radiation flux multiplied by the total surface of the arc (which throws light onto the electrode, on the surface of the metal, and sideways). If we assume that the arc has a cylindrical shape with radius R_{arc} and a height h_{arc}, then the radiation power of one arc will be equal to

$$W_{arc} = S_0 \left(2\pi R_{arc}^2 + 2\pi R_{arc} h_{arc}\right) = 2\pi S_0 R_{arc} \left(R_{arc} + h_{arc}\right).$$

To determine the z component of the radiation flux at a distance r from the radiating cylinder, we consider Fig. 3 from which it is clear that under the arc, when $r < R_{arc}$, the axial component of the flux is equal to

$$S_z = S_0 = \sigma T_{arc}^4\,, \quad r < R_{arc}\,,$$

and with account taken of the axial symmetry, to

$$S_z = 2I_0 \int_0^{\varphi_{max}} d\varphi \int_{\pi/2}^{\theta_{max}} \cos\theta \sin\theta d\theta = -\frac{S_0}{\pi} \varphi_{max} \cos^2\theta_{max} = -S_0 \psi(\varphi, \theta)\,. \tag{15}$$

The angles involved in formula (15) are totally determined (as is seen from Fig. 4) by the running radius of the point of observation, the radius of the arc, and its height:

$$\varphi_{max} = \arcsin\frac{R_{arc}}{r}\,; \tag{16}$$

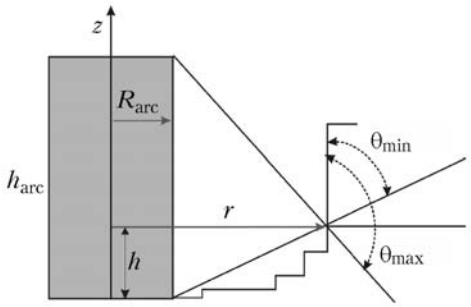

Fig. 5. Determination of the limiting angles of integration.

$$\theta_{max} = \frac{\pi}{2} + \arctan \frac{h_{arc}}{r - R_{arc}}. \tag{17}$$

In the case where the arc has penetrated into the charge the axial component of the radiation flux is found from formula (15), but in this case the maximum angle is

$$\theta_{max} = \frac{\pi}{2} + \arctan \frac{h_{arc} - h}{r - R_{arc}}. \tag{18}$$

The geometric parameters of formula (18) are clear from Fig. 5. In this case the axial component of the flux decreases, since the radiation is determined only by the part of the arc lying above the level of the surface of the charge for this radius.

Now let us consider the radial component of the radiation flux of the arc S_r. We note that the limits of integration by the angle φ are calculated from formula (16). Taking into account the cylindrical symmetry of the problem, from (15) we have

$$S_r = 2I_0 \int_0^{\varphi_{max}} d\varphi \int_{\theta_{min}}^{\theta_{max}} \cos\varphi \sin^2\theta d\theta = 2I_0 \sin\varphi_{max} \int_{\theta_{min}}^{\theta_{max}} \sin^2\theta d\theta = 2S_0 \frac{R_{arc}}{\pi r} \psi,$$

where

$$\psi(\theta_{min}, \theta_{max}) = \frac{\theta_{max} - \theta_{min}}{2} - \frac{1}{2}(\sin\theta_{max}\cos\theta_{max} - \sin\theta_{min}\cos\theta_{min});$$

the limits of iteration by the angle θ are determined (Fig. 5) as $\theta_{min} = \pi/2 - \arctan(h/(r - R_{arc}))$, and θ_{max} are determined from (18). Since the radial fluxes from the arc are expediently determined in the case where the arc penetrates into the charge, it is precisely this case that is given in Fig. 5.

In modeling the distribution of the radiation fluxes from the electrode, we must know the temperature distribution over the end part of the arc-heated electrode and the temperature distribution over the lateral surface of the cylindrical electrode. The calculations yield that the additional contribution of the radiation of the graphite electrode (especially of its end) may amount to ~25% of the contribution of the arc radiation. This is particularly important for numerical modeling of the problem of heating of the charge in the well region, when this region is shielded from the arc radiation by the graphite electrode.

System of Equations of Convective Heat and Mass Transfer in the Molten Bath of an Electric-Arc Steel-Making Furnace. To describe the heat and mass transfer in a molten bath, we suggest using an approach based on diffusion (one-velocity) approximation of the theory of interpenetrating continua [2], which is true at low velocities of relative motion of phases. It is also assumed that at each point one temperature of the medium is determined, and the impact of the mixture's composition manifests itself as the effective coefficients of transfer.

The influence of the blowing of liquid metal with inert gases on heat transfer is accounted for by the effective coefficients of thermal conductivity, i.e., the continuity equation for the gas phase is not considered. Nor will we solve the equation of motion of liquid metal due to free convection, but will use the approximate equations for the velocity components v_r and v_z.

We write the remaining continuity equations for the liquid and solid phases and the energy equation

$$\frac{\partial\left(\varepsilon_{\mathrm{f}}^{\mathrm{m}}\bar{\rho}_{\mathrm{f}}\right)}{\partial\tau}+v_r\frac{\left(\varepsilon_{\mathrm{f}}^{\mathrm{m}}\bar{\rho}_{\mathrm{f}}\right)}{\partial r}+v_z\frac{\partial\left(\varepsilon_{\mathrm{f}}^{\mathrm{m}}\bar{\rho}_{\mathrm{f}}\right)}{\partial z}=\varepsilon_{\mathrm{s}}^{\mathrm{m}}\bar{\rho}_{\mathrm{s}}A_0^{\mathrm{m}},$$

$$\varepsilon_{\mathrm{s}}+\varepsilon_{\mathrm{f}}=1,$$

$$\left[\varepsilon_{\mathrm{f}}^{\mathrm{m}}\bar{\rho}_{\mathrm{f}}C_{p\mathrm{f}}^{\mathrm{m}}+\varepsilon_{\mathrm{s}}^{\mathrm{m}}\bar{\rho}_{\mathrm{s}}C_{p\mathrm{eff}}\right]\frac{\partial T^{\mathrm{m}}}{\partial\tau}+\varepsilon_{\mathrm{f}}^{\mathrm{m}}\bar{\rho}_{\mathrm{f}}C_{p\mathrm{f}}^{\mathrm{m}}v_{\mathrm{r}}\frac{\partial T^{\mathrm{m}}}{\partial r}+\varepsilon^{\mathrm{m}}\bar{\rho}_{\mathrm{f}}C_{p\mathrm{f}}^{\mathrm{m}}v_{\mathrm{z}}\frac{\partial T^{\mathrm{m}}}{\partial z}$$

$$=\frac{\partial}{\partial z}\left[\left(\varepsilon_{\mathrm{s}}\lambda_{\mathrm{s}}+(1-\varepsilon_{\mathrm{s}})\,25.6\lambda_{\mathrm{f}}\right)\frac{\partial T^{\mathrm{m}}}{\partial z}\right]+\frac{1}{r}\frac{\partial}{\partial z}\left[\left(\varepsilon_{\mathrm{s}}\lambda_{\mathrm{s}}+(1-\varepsilon_{\mathrm{s}})\,5.6\lambda_{\mathrm{f}}\right)r\frac{\partial T^{\mathrm{m}}}{\partial r}\right]+Q_{\mathrm{m}}^{\mathrm{chem}},$$

where $Q_{\mathrm{m}}^{\mathrm{chem}}$ = 0.5 MW/m^3 [1];

$$C_{p\mathrm{eff}}=\begin{cases}C_{p\mathrm{s}}^{\mathrm{m}}, & T^{\mathrm{m}}<T_{\mathrm{sol}}^{\mathrm{m}};\\ C_{p\mathrm{s}}^{\mathrm{m}}+\dfrac{Q}{T_{\mathrm{liq}}^{\mathrm{m}}-T_{\mathrm{sol}}^{\mathrm{m}}}, & T_{\mathrm{sol}}^{\mathrm{m}}<T^{\mathrm{m}}<T_{\mathrm{liq}}^{\mathrm{m}};\\ C_{p\mathrm{f}}^{\mathrm{m}}, & T^{\mathrm{m}}>T_{\mathrm{liq}}^{\mathrm{m}};\end{cases}\quad A_0^{\mathrm{m}}=\begin{cases}0, & T^{\mathrm{m}}>T_{\mathrm{sol}}^{\mathrm{m}};\\ \dfrac{1}{T_{\mathrm{liq}}^{\mathrm{m}}-T_{\mathrm{sol}}^{\mathrm{m}}}\dfrac{\partial T^{\mathrm{m}}}{\partial\tau}, & T_{\mathrm{sol}}^{\mathrm{m}}<T^{\mathrm{m}}<T_{\mathrm{liq}}^{\mathrm{m}};\\ 0, & T^{\mathrm{m}}>T_{\mathrm{liq}}^{\mathrm{m}}.\end{cases}$$

It is significant that the initial conditions for $\varepsilon_{\mathrm{s}}^{\mathrm{m}}$ and $\varepsilon_{\mathrm{f}}^{\mathrm{m}}$ have the following form:

$$\varepsilon_{\mathrm{s}}^{\mathrm{m}}(\tau=0)=1-\varepsilon;\quad \varepsilon_{\mathrm{f}}^{\mathrm{m}}(0)=1-\varepsilon_{\mathrm{s}}^{\mathrm{m}}(0)\equiv\varepsilon.$$

The expressions for the effective coefficients of thermal conductivity $(\lambda_{\mathrm{f,eff}})_z$ and $(\lambda_{\mathrm{f,eff}})_r$ have been obtained on the basis of the results of the investigation of turbulent gas jets flowing into the liquid [8]. Such jets occur when air is fed via special nozzles set up in a metallurgical furnace during the mixing of gas and water in the gas-water electrodes, in systems protecting water reserves from penetration of oils and petroleum, etc. into them. When the gas is released upward into the motionless liquid. there develops a vertical ascending jet which disintegrates into bubbles quickly formed near the nozzle. In [8] it is shown that it is possible to obtain the dependence of the average velocity of ascent of the bubbles and of the average velocity (and the velocity on the axis) of the jet on the rate of gas flow through the nozzle.

Let us assume that the flow in a gas-liquid jet is similar to the flow in a porous body where, as is known (see, e.g., [3]), the thermal conductivities are effective quantities reflecting the presence of additional effects that are linked to a substantial transfer of heat due to a random mixing caused by an irregular packing of the particles of a porous medium and by the irregularity of flow (pseudoturbulence). These dispersion effects result in a significant increase in the effective thermal conductivity, with heat conduction becoming an anisotropic quantity, since the dispersion effects are the most pronounced in the direction of filtration. For a porous body made up of spherical particles with a diameter d, it is suggested [3, 6] that the following equations for $\lambda_{\mathrm{f,eff}}$ be used

$$(\lambda_{\mathrm{f,eff}})_z=\lambda_{\mathrm{f}}\left(\bar{\varepsilon}_{\mathrm{f}}+0.5\mathrm{Pe}\right),\quad (\lambda_{\mathrm{f,eff}})_r=\lambda_{\mathrm{f}}\left(\bar{\varepsilon}_{\mathrm{f}}+0.1\mathrm{Pe}\right),$$

where $\bar{\varepsilon}_{\mathrm{f}}=1-\bar{\varepsilon}_{\mathrm{g}}$ is the volume concentration of the liquid phase ("porosity") and $\mathrm{Pe}=\mathrm{PrRe}=\dfrac{|\Delta v|f\rho_{\mathrm{f}}c_{\mathrm{f}}}{\lambda_{\mathrm{f}}}$. For the ascending velocity of bubbles $|\Delta v|\approx 0.1$ m/sec, Pe $\approx$ 50, and $\bar{\varepsilon}_{\mathrm{f}}\approx 0.55$, we obtain

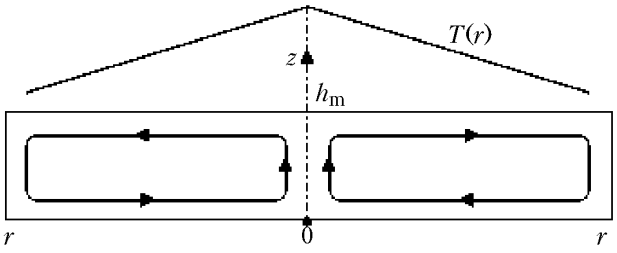

Fig. 6. Diagram of free-convective flow.

$$(\lambda_{f,eff})_z \approx 25.6\lambda_f, \quad (\lambda_{f,eff})_r \approx 5.6\lambda_f .$$

As is noted in [9], in rectangular two-dimensional regions nonuniformly heated from above, we have cellular convection at any values of the Grashof number Gr = $g\beta\Delta T/\nu_*^2$. It has been shown that in the stationary case for $\frac{h_m}{2R} < 1$ intense convective motion has a cellular structure and covers the entire region. The extremum in the temperature distribution on the upper surface corresponds to the boundary between the basic cells. The fluid will ascend at the center of the region and descend at the lateral boundaries (Fig. 6). It will be heated at the upper wall and be cooled at the lateral boundaries and the lower base, i.e., at the upper wall, the fluid flows opposite to the temperature gradient. Thus, convection contributes to the heating of the upper fluid layers lying near the heated upper boundary and to its cooling in the lower layers; when the convection intensity is sufficiently high, the temperature of the lower fluid layers will decrease so that it will become lower than the temperature corresponding to the heat-conduction regime. For Gr $\le 10^3$, the convection intensity is in direct proportion to the value of Gr. As Gr increases further, the convective-motion velocity grows more slowly. We note that in heating from above, the convection intensity is approximately 1.8 times lower than in heating from the side and 1.5 times lower than in heating from below. For $\frac{h_m}{2R} > 1$, intense convective motion is concentrated only in the upper layers near the heating zone. The fluid layers lying lower remain virtually quiescent.

Heat exchange in free convection in a closed horizontal plane with adiabatic horizontal walls and differently heated end walls has been investigated theoretically in [10]. The approximate expressions for the velocity distributions in closed plane cavities are proposed. The flow structure is characterized by two basic regions: the central region with a parallel counterflow in which a more heated fluid occupies the upper half of the cross section, and the end region with a length of the order of h_m or smaller in which the parallel branches of the counterflow are rotated through 180°. Here we assume that the molten bath has a cylindrical syttemtry. On the nonuniformly heated surface, the highest temperature value corresponds to the central parts; therefore, we will consider half of the cross section ($0 \le r \le R$, $0 \le z \le h_m$). We assume the following approximate expressions for the velocity components in the form of the products of expressions dependent on r and z:

$$v_r = -u_0 \frac{r}{\delta}\left(\frac{R-r}{\delta}\right)^3\left[\frac{1}{4}\left(\frac{R-r}{\delta}\right)+\frac{1}{3}\right]\left[\frac{1}{6}\left(\frac{z}{h_m}\right)^3-\frac{1}{4}\left(\frac{z}{h_m}\right)^2+\frac{1}{12}\frac{z}{h_m}\right]\frac{1}{\psi_n} \equiv -u_0\frac{\varphi_1(r)\,\varphi_2(z)}{\psi_n}, \tag{19}$$

$$v_z = -u_0\frac{h_m}{12\delta}\left(\frac{R-r}{\delta}\right)^2\left[\frac{r}{\delta}\left(1+\frac{R-r}{\delta}\right)-2\left(\frac{R-r}{\delta}\right)\left(\frac{1}{4}\frac{R-r}{\delta}+\frac{1}{3}\right)\right]$$

$$\times\left[\frac{1}{2}\left(\frac{z}{h_m}\right)^4-\left(\frac{z}{h_m}\right)^3+\frac{1}{2}\left(\frac{z}{h_m}\right)^2\right]\frac{1}{\psi_n} \equiv -u_0\frac{f_1(r)\,f_2(z)}{\psi_n}, \tag{20}$$

where $\psi_n = \max\{\varphi_1(r)\varphi_2(z);\ f_1(r)f_2(z)\}$;

$$u_0 = \sqrt{g\beta\Delta T h_{\rm m}} \tag{21}$$

is the characteristic velocity of free-convective flow in the case where viscous, inertial, and body forces are the quantities of one order [11], $\beta \approx 1.5\cdot 10^{-4}$ 1/K, ΔT is the characteristic temperature difference between the surfaces $r = 0$ and $r = R$, δ is the length of the end region ($\delta \approx 0.6 h_{\rm m}$), and $h_{\rm m} = h_{\rm m}(\tau)$. These distributions satisfy the continuity equation

$$\frac{\partial (rv_r)}{\partial r} + \frac{\partial (rv_z)}{\partial z} = 0 ,$$

and the zero boundary conditions at $z = 0$ and $z = h_{\rm m}$; furthermore, we have $v_r = 0$ for $r = R$, $r = 0$, and $z = \frac{1}{2} h_{\rm m}$, and $v_z = 0$ for $r = R$.

The initial conditions of the problem are as follows: $T_{\rm s}(r, z, 0) = 300$ K, $T_{\rm g}(r, z, 0) = 2000$ K, $h_{\rm m}(\tau = 0) = 0.1$ m, $h_{\rm s}(\tau = 0) = 1.9$ m, $\varepsilon_{\rm s}^{\rm m}(\tau = 0) = 1 - \varepsilon$, and $\varepsilon_{\rm f}^{\rm m}(\tau = 0) = \varepsilon$.

The boundary conditions of the problem are as follows:

for the cooled roof $z = h_{\rm s}(\tau)$, $R > r > R_{\rm w}$

$$\lambda_{\rm s,eff} \frac{\partial T_{\rm s}}{\partial z} = -\sigma \varepsilon_{r\rm eff} \left[T_{\rm s}^4 - T_{\rm r}^4\right] - 0.6 \sqrt{2 \frac{\overline{R}}{\overline{M}} T_{\rm s}} \sqrt{\frac{\rho_\infty}{\rho_{\rm e}(T_{\rm s})}} (\rho_{\rm e} - \rho_\infty) Q_{\rm sub} + S_0 \psi ;$$

for $z = h_{\rm m}(\tau)$, $R > r > R_{\rm w}$

$$T_{\rm s} - T^{\rm m} = \frac{\partial T_{\rm s}}{\partial z} \frac{\lambda_{\rm s} \delta_{\rm sl}}{\lambda_{\rm sl}} , \quad \delta_{\rm sl} \approx h_{\rm met} ;$$

$$\lambda^{\rm m} \frac{\partial T^{\rm m}}{\partial z} - \lambda_{\rm s,eff} \frac{\partial T_{\rm s}}{\partial z} = \overline{\rho}_{\rm f} C_{p\rm f} T_{\rm liq} \frac{dh_{\rm m}}{d\tau} ; \quad \overline{\rho}_{\rm f} \frac{dh_{\rm m}}{d\tau} = \frac{2(1-\varepsilon)\overline{\rho}_{\rm s} \int_{h_{\rm m}}^{h_{\rm s0}} \int_0^R A_0 r dr dz}{\varepsilon R^2} ;$$

$$\tau = R_{\rm w} , \quad -\lambda_{\rm s,eff} \frac{\partial T_{\rm s}}{\partial r} = S_0 \psi ;$$

$$r = R , \quad \frac{\partial T_{\rm s}}{\partial r} = 0 ;$$

$$r = R(z) , \quad \frac{\partial T^{\rm m}}{\partial \mathbf{n}} = 0 ;$$

$$z = 0 ; \quad \frac{\partial T^{\rm m}}{\partial z} = 0 ,$$

where $\mathbf{n}$ is the unit vector of the external normal to the furnace surface, $h_{\rm met} = 3\cdot 10^{-3} I_{\rm arc}$ mm is the height of penetration of the arc into the metal, and $I_{\rm arc}$ is the current strength.

Description of the Program and Algorithm of Calculation of Heat Exchange in Melting in the Electric-Arc Steel-Making Furnace. The above-described model of heating and melting of the charge in an electric-arc steel-making furnace is realized in the form of a software system in which the basic physical processes are taken into account in a two-dimensional axisymmetric formulation with the use of the principle of splitting by physical processes. The parameters describing the system's state are successively varied on each time step. The contribution of each of the

physical processes which are allowed for determines the total change in the parameters of the system. In our model, one possible order is as follows: calculation of the volume sources of energy release due to the chemical reactions in the charge and the melt, allowance for the heat exchange with gases in the region of the charge, calculation of the velocity field in the marsh region, calculation of the motion of the boundary between the melt and the charge, and calculation of the transfer of heat in the region of the marsh and the charge. The order of calculation of the contributions is usually assumed to be unimportant but it is expedient to select a natural order: first to calculate the volume sources and then to determine the mass and energy redistribution due to the transfer processes. Taking into account that in our case the problem is nonlinear (the parameters of the medium and the boundary conditions are temperature-dependent), in selecting the time step, we must impose a restriction on the change in the temperature, even in the case of absolutely stable implicit difference schemes. In the procedure developed, we use the finite-difference flux-marching method [12, 13].

For direct description of the parameters in the region of the charge and the melt, we introduce the specific enthalpy of a unit volume, which is unambiguously related to the temperature, the porosity, and the volume fractions of the solid and liquid phases in a one-temperature equilibrium approximation. The position of the boundaries of melting is determined by the volume fraction of the solid phase in a spatial cell. Each spatial cell is described by the specific enthalpy, the temperature, the porosity, and the volume fraction of the solid and liquid phases. The belonging of the cells to the melt or to the charge is described by assigning the medium's porosity ε and the index of the cell along the z axis marking the boundary between the marsh and the charge. We take thus far $\varepsilon = 0$ in the marsh region (the cell is totally filled with metal), $\varepsilon = 1 - \rho_s/\overline{\rho}_s$ in the charge region (the cell is partially filled with metal, partially with gas), and $\varepsilon = 1$ in the well region (the cell contains no metal). In the charge region, the medium's porosity is assumed to be constant, until the volume fraction of the solid phase in the cell becomes equal to $\varepsilon_s = 0$, i.e., partial discharge of the melt is disregarded in the process of melting of the cells belonging to the charge. In the case where the cell belonging to the charge becomes completely melted we redetermine the well boundaries; the mass and enthalpy of the melted cells are transferred to the melt surface and the porosity in these cells is taken to be $\varepsilon = 1$. Thus, the formation of a well in the charge and the rise of the melt level are described in finite-difference form with allowance for the conservation of mass and energy.

The process of melting is unambiguously determined by the cell's specific enthalpy, which is related to the volume fraction of the solid phase in the cell. With variation in the temperature it linearly decreases from the solidus temperature T_{sol} to the liquidus temperature T_{liq} and is equal to $\varepsilon_s = 1$ at $T \le T_{sol}$ and $\varepsilon_s = 0$ at $T \ge T_{liq}$.

The motion of the boundary of melting of the charge is determined in the program not only by the formation of the well under the arc but is is also determined by the mechanism of falling of the charge onto the marsh surface. The reason is that at the instants the arc reaches the marsh surface, the charge cells located in the lower lateral part of the well next to the arc melt. Since the melt from this region flows down into the marsh, the upper computational cells shift downward to the marsh surface.

As the calculations have shown, the intense convective transfer of heat forms the region of completely molten metal in the marsh under the charge. In this case the cells of the partially unmelted marsh and charge above the melted region must descend under gravity, displacing the melt upward, i.e., we must have a descent of the charge into the marsh. This is also taken into account in the program when the motion of the charge boundary and the rise of the marsh level are determined. We note that the rise of the marsh level is allowed for discretely in the program. Filling of the cell layer in the well and charge region adjacent to the marsh is carried out only when the integral volume of the melted cells is capable of filling the entire layer. Naturally, the layer is filled with allowance for the conservation of mass and energy: in the well region, the cells are filled completely, whereas in the charge region, they are filled with allowance for porosity. It is noteworthy that the arc motion in the process of formation of the wall is described in a natural manner, i.e., the arc is always tied to the well bottom or to the molten-bath surface, when the arc descends to the marsh level.

The temperature dependences of the medium's thermophysical parameters can be assigned in the form of functional dependences or tables. To allow for the temperature dependence of the thermophysical parameters (thermal conductivities, specific heats, and volume fractions of the melt and the solid phase) on each time step the iteration procedure allowing for their change is provided. This procedure allows for the change in the temperature-dependent boundary conditions (radiation fluxes at the boundaries and heat exchange with the furnace walls), too. Since we do not

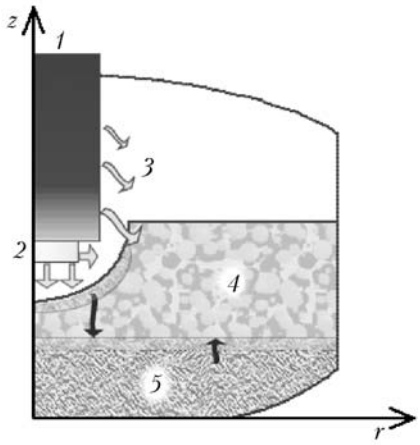

Fig. 7. Geometric scheme of the problem: 1) electrode; 2) arc; 3) radiation;

model the process on a full scale (with calculation of the dynamics of heating of the walls and the furnace roof) in the problem, radiation heat exchange between the marsh and the charge is allowed for by assignment of the time-constant temperature T_r. Depending on whether the spatial cells belong to the region of the charge or the marsh (Fig. 7), in the calculations, we take into account different physical processes describing the dynamics of melting in electric-arc steel-making furnaces.

To save computational time and resources we carry out numerical modeling with allowance for the axial symmetry only in half the region. The computational procedure is tried out for a cylindrical geometry of the furnace without allowance for the geometry of the bottom part. In the calculations, the spatial grid is 300 × 200 nodes along the r and z axes respectively. A spatial step is assigned constant and equal to $\Delta z_i = \Delta r_j = 1$ cm. With allowance for the characteristics thermophysical parameters of the melt and the charge, such a spatial grid is a minimum grid required for fulfillment of the conditions of approximation of the distributions of the temperature and the volume fractions of the melt and the solid phase.

We should make a remark which is of decisive importance in describing the dynamics of melting of the charge in an electric-arc steel-making furnace. As the test calculations have shown, the initial phase of formation of the well is fairly short and lasts a few minutes (depending on the characteristic arc temperature). Heat transfer through the boundary between the charge and the marsh does not ensure melting of the charge cells adjacent to the marsh surface. Once the well has been fused, further melting of the charge is ensured by the lateral emission of the arc and the electrode. We have the melting of the charge cells in the region adjacent to the melt surface. Since in the computational algorithm, the melted charge cells are transferred to the marsh, ensuring a rise of its level, it is natural that the overlying cells of unmelted charge fall down onto the marsh surface. This physically clear fact is rather difficult to describe mathematically but algorithmically this process is realized on the basis of an analysis of the cells in the charge region by calculation of the melted-cell volume and energy, by transfer of the overlying cells to the site of the melted ones, and by redetermination of the upper boundary of the charge (geometry of the charge boundary).

The initial conditions correspond to the initially cold charge ($T(r,\ 0 < z < h_{m0},\ \tau = 0) = 300$ K) above the melt region h_{m0}. In the marsh, the volume fraction of the solid phase is initially assigned equal to the charge porosity, which uniquely determines the specific enthalpy and the initial temperature of the marsh under equilibrium conditions.

Results of Numerical Modeling of the Process of Melting of Metal Scrap. As an example of numerical modeling of melting in an electric-arc steel-making furnace we give results of calculation of charge melting in a cylindrical furnace of radius 3 m under the action of the arc with a characteristic arc temperature of 4800 K, an effective radius of 64 cm, and a height of 17.3 cm. Such parameters of the arc correspond to an electric three-arc steel-making furnace with radiation power of each arc $W_{arc} \approx 32.7$ MW. The given versions of calculations refer to the case of heat-insulated lateral surfaces of the electric-arc steel-making furnace.

The thermophysical parameters of the metal are assigned in accordance with the data of [1]: the specific heats of the solid and liquid phases are set temperature-independent and equal to $C_s = 710$ J/(kg·K) and $C_{f_3} = 824$ J/(kg·K); $T_{sol} = 1693$ K and $T_{liq} = 1743$ K; $Q = 0.274$ MJ/kg; the density of the solid phase is 7800 kg/m^3 and that of the

TABLE 1. Characteristics of Charge Types

Type of charge	ε_{ch}	ρ_{ch}, kg/m^3	ε_{s0}^m	T_0^m, K	m_{ch}, tons	m_s^m, tons
Recycled scrap	0.769	1802	0.231	1744	96.7	5.1*
A10 packets	0.909	798	0.091	1754	38.13	2**

*The marsh mass is 20.3 tons.

**The marsh mass is 20 tons.

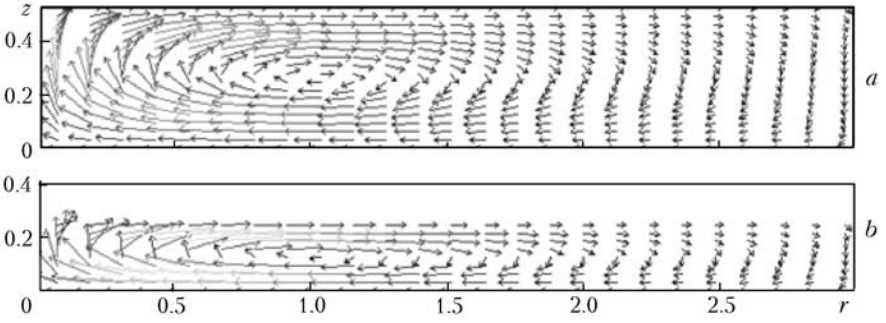

Fig. 8. Vector of velocities of free-convective mixing in the bath by the instant of completion of the melting: a) recycled scrap; b) A10 packets.

liquid phase is 7000 kg/m^3; the coefficient of thermal conductivity for the solid and liquid phases are also set temperature-independent and equal to λ_s = 70 W/(m·K) and λ_f = 35 W/(m·K); the emissivities of the charge and the marsh are assumed to be temperature-independent and equal to ε_r = 0.9; the initial height of the charge layer is equal to 1.9 m, and the initial height of the marsh is 0.1 m. The calculations are carried out for two characteristic kinds of charge whose parameters are given in Table 1.

In numerical modeling, we allow for the contribution of the emission of the graphite electrode in addition to the arc emission. The emissivity of graphite is set temperature-independent and equal to 0.9. The temperature distribution over the electrode surface is assigned from the results of our numerical modeling corresponding to the stationary regime of arcing, i.e., the dynamics of heating of the graphite electrode is disregarded, since the main contribution to the radiation flux is made by the end electrode portion where a nearly stationary temperature distribution is established by 10 min, as the calculations have shown. Such an approach to allowance for the electrode contribution is quite justified. The phase of fusion of the well by the arc (which lasts 1 to 2.5 min) is followed by the phase of heating of the melt and of melting and falling-down of the well walls. The walls are melted mainly in the region of contact of the lateral well wall with the melt.

To explain the modeling (realized in the software system) of the mechanism of motion of the boundary of the charge in its melting and descending into the molten bath we give results of numerical modeling of the melting of recycled scrap, when

(1) allowance is made for the melting of the charge and the fall of the lateral well walls on the marsh surface disregarding free-convective mixing (u_0 = 0);

(2) the rate of free-convective mixing is determined by the average temperature difference on the axis and walls of the electric-arc steel-making furnace from formula (21); the dynamics of the charge boundary is also determined only by the fall of the charge on the melt surface;

(3) the descent of the charge into the molten bath, when the charge-filled cells overlay the completely melted layers, is allowed for additionally.

It is noteworthy that in the first case, which corresponds to the model considered in [1], allowance only for the heat conduction in the molten bath does not give satisfactory results (even if we start from the effective coefficients of thermal conductivity allowing for the transfer of radiation in the charge and for bottom blowing in the marsh). The metal is strongly overheated in the region above the arc and most of the charge remains unmelted over a period of ~1 h. In this case well formation is determined only by the radial component of the flux of arc and elec-

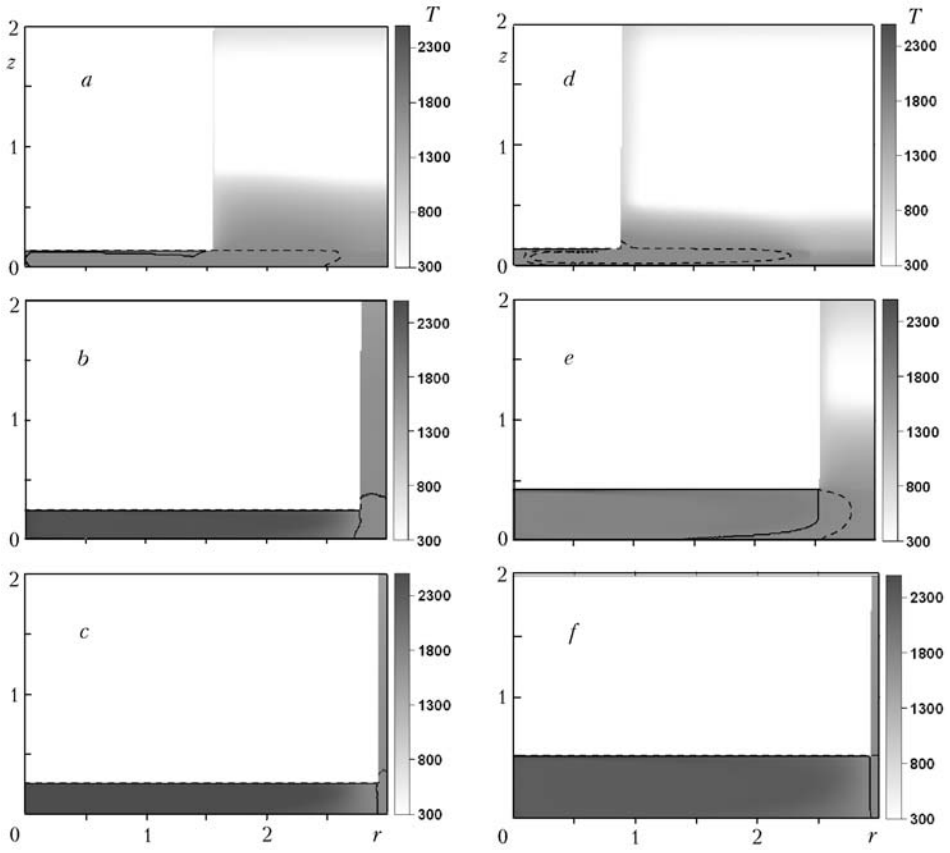

Fig. 9. Dynamics of melting in the electric-arc steel-making furnace for different types of charge: a–c) recycled scrap; d–f) A10 packets (a and d) τ = 1, b and e) 30, c and f) 60 min; solid curve, the volume fraction of the liquid phase is ε_f = 1, dashed curve, ε_f = 0.5). r, z, m; T, K.

trode radiation. The charge cells next to the arc are melted at the melt surface. The temperature in the region of the arc spot on the marsh surface grows quite rapidly to values corresponding to the radiation flux of the arc, and the energy contribution to the system sharply drops. The efficient heat removal from the region of the arc spot can be ensured only by the mechanism of convective mixing of the molten bath. The above fact is taken into account, in the model, by introducing convective terms described by the model fraction (19) and (20) into the equation of heat conduction in the molten bath.

The fields of velocity-vector distribution in the molten bath (which correspond to the end of the process in the case of melting of recycled scrap and A10 packets) are given in Fig. 8. In numerical modeling, the maximum value of the velocity vector is determined on each time layer by the average temperature difference on the axis and at the wall of the furnace (see (21)). The velocity of convective mixing grows from zero to the maximum values $u_0 \approx$ 0.5–0.7 m/sec in the process of melting. In [14], a value of the maximum velocity of ~1 m/sec is given for furnaces of constant current 50 kA; therefore, the employed value of the characteristic convection velocity cannot be thought of as being overstated.

Figure 9 shows the temperature fields and the isolines of volume fraction of the solid phase for melting of recycled scrap and A10 packets for an effective radiation power of the arc of 98.1 MW. After the phase of melting of the well, the arc reaches the bath surface and the phase of melting of the bath under the arc begins. Its duration for the lighter scrap is shorter, just as the duration of the phase of melting of the well. For the recycled scrap, the molten bath under the arc is completely melted by an instant of ~20 min, whereas for the A10 packets it is melted by ~10 min. The charge-melting rate drops with distance from the well axis, since the radial component of the radiation flux from the arc and the lateral electrode surface is diminished. In the region of complete melting, the temperature continues to grow but is distributed quite uniformly owing to convective mixing.

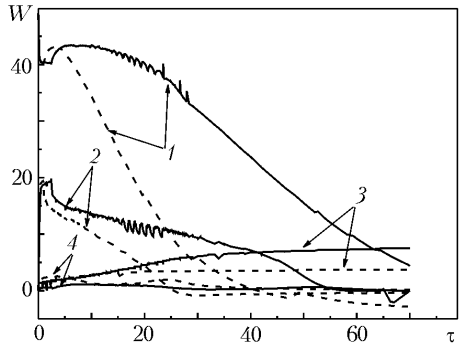

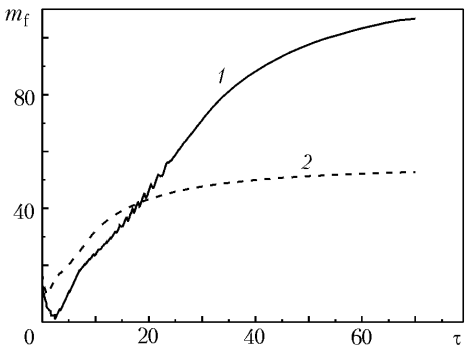

Fig. 10. Integral powers of energy release from the arc and the electrode (radial W_r and axial W_z) and due to the chemical reactions in the charge (W^{chem}) and in the molten bath W_m^{chem}) for melting of recycled scrap (solid curves) and A10 packets (dashed curves) in the electric-arc steel-making furnace vs. time: 1) W_z; 2) W_r; 3) W^{chem}; 4) W_m^{chem}. W, MW; τ, min.

Fig. 11. Molten-metal mass vs. time: 1) recycled scrap; 2) A10 packets. m_f, tons; τ, min.

Figure 10 plots the power of the energy contribution of the components of radiation fluxes (W_z and W_r), the power of the chemical reaction of scaling in the charge (W^{chem}), and the power of chemical reactions in the molten bath (W_m^{chem}) as functions of the time for melting of recycled scrap and A10 packets by an arc with an effective radiation power of 98 MW. The chemical reactions in the molten bath are taken into account by assignment of a constant volume power of heat release of 0.5 MW/m^3 (according to the recommendations of [1]). This component grows linearly with molten-bath volume and attains a constant value late in the melting, when the melting rate drops, as the distance between the lateral well walls and the arc increases. The values of the radiation-power components behave nonmonotonically with time. At the stage of melting of the well, the z component of the flux is constant and amounts to ~40% of the effective arc power. The radial component W_r grows from zero to 20 MW in this period because of the penetration of the arc and the electrode into the fused well. Once the melt surface has been reached by the arc, the z component begins to grow due to the increase in the free area of the molten bath in melting of the lateral well walls, whereas the radial component begins to drop. The z component of the flux remains virtually constant in the period of melting under the arc but subsequently decreases with growth in the melt temperature under the arc. At these instants, the radial component diminishes due to the melting of the lateral well walls, their movement away from the arc, and growth in the temperature of the charge of the lateral well walls.

Because of the nonuniformity of heating of the well (elevated temperatures of the bath under the arc and slow melting of the charge and the marsh in peripheral regions of the furnace), the model allowing for the spatial temperature distribution gives significant differences in energy balance compared to one-dimensional or balance models. Melting according to the balance model must be completed by an instant of time of 38 and 16 min for the case of recycled scrap and A10 packets respectively. However, because of the nonuniformity of the temperature distribution and overheating of the marsh under the arc, a major portion of the charge remains unmelted by these instants. This is quite evident from Fig. 11, where the mass of the molten metal is plotted as a function of the time for the cases of melting of recycled scrap and A10 packets.

Conclusions. We have developed the mathematical model of heat and mass transfer in heating and melting of metal scrap in an electric-arc steel-making furnace based on the theory of interpenetrating continua. The fundamental importance of the lateral arc- and electrode-radiation fluxes determining the heating of the melt and the melting of the lateral charge wall in the region adjacent to the melt surface has been noted.

The numerical modeling of the problem has shown that the mechanism of heat conduction, even with effective coefficients (allowing for the transfer of radiation in the charge and for bottom blowing in the marsh) does not give results adequate to the technological process. The surface temperature of the melt in the region of the arc spot rapidly grows to values corresponding to the radiation flux of the arc, and the energy contribution of the system

sharply drops. Efficient heat removal from the region of the arc spot can be ensured only by the mechanism of convective mixing of the molten bath.

NOTATION

C_p, specific heat at constant pressure, J/(kg·K); d, diameter of a bubble, m; d_s, equivalent diameter of a solid scrap particle, m; E, activation energy, J/mole; Gr, Grashof number; g, free-fall acceleration, m/sec^2; ΔH, scaling-reaction heat, J/mole; h, running value of the arc height, m; h_m, marsh height, m; h_{arc}, arc height, m; h_s, upper boundary of the scrap, m; $\mathbf{I}_\nu$, radiation intensity, W/(m^2·sr); I_{arc}, current strength, A; $\overline{M}$, molecular weight; m, mass, kg; Pe, Péclet number; Pr, Prandtl number; Q, melting heat, J/kg; Q_{sub}, sublimation heat, J/kg; R, radius of the furnace, m; r, z, coordinates, m; R_{sp}, radius of the spot, cm; R_{arc}, equivalent radius of the spot of the heat source, m; $\overline{R}$, universal gas constant, J/(mole·K); Re, Reynolds number; S, specific surface, m^{-1}; T, temperature, K; ΔT, temperature difference over the bath width, K; T_*, heated-gas temperature, K; T_{sol} and T_{liq}, solidus and liquidus temperatures, K; V, volume, m^3; v_r and v_z, velocity components, m/sec; $\mathbf{W}$, radiation flux, W/m^2; W, integral power, W; w, filtration velocity, m/sec; α_m, parameter, m^6/kg^2; α_ν, coefficient of internal heat exchange, W/(m^3·K); β, coefficient of volumetric expansion of the fluid, K^{-1}; δ_{sl}, thickness of the slag layer, m; ε, porosity; ε_r, emissivity; ε^m, volume fractions of phases in the marsh; θ and φ, angles determining the direction of the beam; λ, thermal-conductivity coefficient, W/(m·K); μ, coefficient of dynamic viscosity, N·sec/m^2; ν, frequency, sec^{-1}; ν_*, coefficient of kinematic viscosity, m^2·sec^{-1}; $\overline{\rho}$, true density, kg/m^3; ρ_{ch}, bulk density of the charge, kg/m^3; σ, Stefan–Boltzmann constant, W/(m^2·K^4); τ, time, sec; ψ, angular coefficient; ψ_n, normalization factor; Ω, solid angle, sr. Subscripts and superscripts: eff, effective; g, gas; f, fluid; s, solid phase; m, marsh; arc, arc; in, internal; sp, spot; sl, slag; w, well; chem, chemical; met, metal; 0, initial; n, normalization; ch, charge; sol, solidus; liq; liquidus; r, roof; sub, sublimation; max, maximum; min, minimum; e, saturated steam.

REFERENCES

1. V. I. Timoshpol'skii, Yu. V. Feoktistov, A. B. Steblov, et al., *Thermal Technology of Metallurgical Miniplants* [in Russian], Navuka i Tékhnika, Minsk (1992).
2. R. I. Nigmatulin, *Principles of the Mechanics of Heterogeneous Media* [in Russian], Nauka, Moscow (1978).
3. N. V. Pavlyukevich, *Introduction to the Theory of Heat and Mass Transfer in Porous Media* [in Russian], ITMO NAN Belarusi, Minsk (2002).
4. Yu. A. Samoilovich, V. I. Timoshpol'skii, I. A. Trusova, and V. V. Filippov, *Steel Ingot* [in Russian], Vol. 2, Balaruskaya Navuka, Minsk (2000).
5. V. Yu. Bolotov, O. I. Pavlyuchenkov, V. I. Timoshpol'skii, et al., A three-dimensional mathematical model of thermal operation of an electric-arc steel-melting furnace by the top-level technology, *Énergetika*, No. 1, 72–79 (2002).
6. A. Amiri and K. Vafai, Analysis of dispersion effects and non-thermal equilibrium, non-Darcian, variable porosity incompressible flow through porous media, *Int. J. Heat Mass Transfer*, **37**, No. 6, 939–954 (1994).
7. S. I. Gertsik and V. A. Vladimirov, Distribution of heat fluxes over the surface of a metal in an electric-arc furnace in the period of liquid bath, *Steel*, No. 1, 28–31 (1998).
8. G. N. Abramovich (Ed.), *Theory of Turbulent Jets* [in Russian], Nauka, Moscow (1984).
9. A. V. Luikov and B. M. Berkovskii, *Convection and Thermal Waves* [in Russian], Énergiya, Moscow (1974).
10. A. Bejan and T. Twen, Free convection laminar heat transfer in a horizontal closed cavity with differently heated end walls, *Heat Transfer*, No. 2, 87–94 (1978).
11. Yu. A. Sokovishin and O. G. Martynenko, *Introduction to the Theory of Free-Convective Heat Transfer* [in Russian], LGU, Leningrad (1982).
12. R. P. Fedorenko, *Introduction to Computational Physics* [in Russian], Izd. MFTI, Moscow (1994).
13. A. A. Samarskii and Yu. P. Popov, *Difference Methods of the Solution of Gas Dynamics Problems* [in Russian], Nauka, Moscow (1980).
14. I. M. Yachikov, O. I. Karandaeva, T. P. Larina, and I. V. Portnova, *Simulation of Electromagnetic Processes in Direct Current Electric Arc Furnaces* [in Russian], G. I. Nosov MGTU Izd. Tsentr, Magnitogorsk (2005).